where K_m is the eddy viscosity in the ocean (assumed constant). As a lower boundary condition assume that $u, v \to 0$ as $z \to -\infty$. If $K_m = 10^{-3}\ \mathrm{m^2\ s^{-1}}$ what is the depth of the surface Ekman layer at 45°N latitude?

5.7. Show that the vertically integrated mass transport in the wind-driven oceanic surface Ekman layer is directed 90° to the right of the surface wind stress in the Northern Hemisphere. Explain this result physically.

5.8. A homogeneous barotropic ocean of depth $H = 3$ km has a zonally symmetric geostrophic jet whose profile is given by the expression

$$u_g = U \exp[-(y/L)^2]$$

where $U = 1\ \mathrm{m\ s^{-1}}$ and $L = 200$ km are constants. Compute the vertical velocity produced by convergence in the Ekman layer at the ocean bottom and show that the meridional profile of the secondary cross-stream motion forced in the interior is the same as the meridional profile of u_g. What are the maximum values of v and w if $K_m = 10^{-3}\ \mathrm{m^2\ s^{-1}}$ and $f = 10^{-4}\ \mathrm{s^{-1}}$? (Assume that w and the eddy stress vanish at the surface.)

5.9. Using the approximate zonally averaged momentum equation

$$\frac{\partial \bar{u}}{\partial t} \cong f\bar{v}$$

compute the spin-down time for the zonal jet in Problem 5.8.

5.10. Derive a formula for the vertical velocity at the top of the planetary boundary layer using the mixed-layer expression (5.22). Assume that $|\bar{\mathbf{V}}| = 10\ \mathrm{m\ s^{-1}}$ is independent of x and y and that $\bar{u}_g = \bar{u}_g(y)$. If $h = 1$ km what value must κ_s have if the result is to agree with the vertical velocity derived from the Ekman layer solution with $De = 1$ km?

5.11. Show that $K_m = kzu_*$ in the surface layer.

Suggested References

Arya, *Introduction of Micrometeorology*, gives an excellent introduction to boundary layer dynamics and the elements of turbulence at the beginning undergraduate level.

Sorbjan, *Structure of the Atmospheric Boundary Layer*, is a monograph that provides a good survey of the current state of boundary layer research at the graduate level.

Panofsky and Dutton, *Atmospheric Turbulence*, has a good graduate level treatment of the statistical properties of turbulence, as well as engineering applications.

Stull, *An Introduction to Boundary Layer Meteorology*, provides a comprehensive and very nicely illustrated treatment of all aspects of the subject at the beginning graduate level.

Chapter

6 Synoptic-Scale Motions I: Quasi-geostrophic Analysis

A primary goal of dynamic meteorology is to interpret the observed structure of large-scale atmospheric motions in terms of the physical laws governing the motions. These laws, which express the conservation of momentum, mass, and energy, completely determine the relationships among the pressure, temperature, and velocity fields. As we saw in Chapter 2, these governing laws are quite complicated even when the hydrostatic approximation (which is valid for all large-scale meteorological systems) is applied. For extratropical synoptic-scale motions, however, the horizontal velocities are approximately geostrophic (see Section 2.4). Such motions, which are usually referred to as *quasi-geostrophic*, are simpler to analyze than are tropical disturbances or planetary-scale disturbances. They are also the major systems of interest in traditional short-range weather forecasting and are thus a reasonable starting point for dynamical analysis.

In this chapter we show that for extratropical synoptic-scale systems the twin requirements of hydrostatic and geostrophic balance constrain the baroclinic motions so that to a good approximation the structure and evolution of the three-dimensional velocity field are determined by the

distribution of geopotential height on isobaric surfaces. The equations that express these relationships constitute the quasi-geostrophic system. Before developing this system of equations it is useful to summarize briefly the observed structure of midlatitude synoptic systems and the mean circulations in which they are embedded. We then develop the quasi-geostrophic momentum and thermodynamic energy equations and show how these can be manipulated to form the *quasi-geostrophic potential vorticity equation* and the *omega equation*. The former equation provides a method for predicting the evolution of the geopotential field, given its initial three-dimensional distribution; the latter provides a method for diagnosing the vertical motion from the known distribution of geopotential. In both cases alternative versions of the equations are discussed to help elucidate the dynamical processes responsible for the development and evolution of synoptic-scale systems.

6.1 The Observed Structure of Extratropical Circulations

Atmospheric circulation systems depicted on a synoptic chart rarely resemble the simple circular vortices discussed in Chapter 3. Rather, they are generally highly asymmetric in form with the strongest winds and largest temperature gradients concentrated along narrow bands called *fronts*. Also, such systems generally are highly baroclinic; the amplitudes and phases of the geopotential and velocity perturbations both change substantially with height. Part of this complexity is due to the fact that these synoptic systems are not superposed on a uniform mean flow but are embedded in a slowly varying planetary-scale flow that is itself highly baroclinic. Furthermore, this planetary-scale flow is influenced by *orography* (that is, by large-scale terrain variations) and continent–ocean heating contrasts, so that it is highly longitude dependent. Therefore, it is not accurate to view synoptic systems as disturbances superposed on a zonal flow that varies only with latitude and height. As is shown in Chapter 8, however, such a point of view can be useful as a first approximation in theoretical analyses of synoptic-scale wave disturbances.

Zonally averaged cross sections do provide some useful information on the gross structure of the planetary-scale circulation, in which synoptic-scale eddies are embedded. Figure 6.1 shows meridional cross sections of the longitudinally averaged zonal wind and temperature for the solstice seasons of (a) December, January, February (DJF) and (b) June, July, August (JJA). These sections extend from approximately sea level (1000 mb) to about 16 km altitude (100 mb). Thus the entire troposphere is shown while the lower stratosphere is shown only for the extratropical regions. In the present

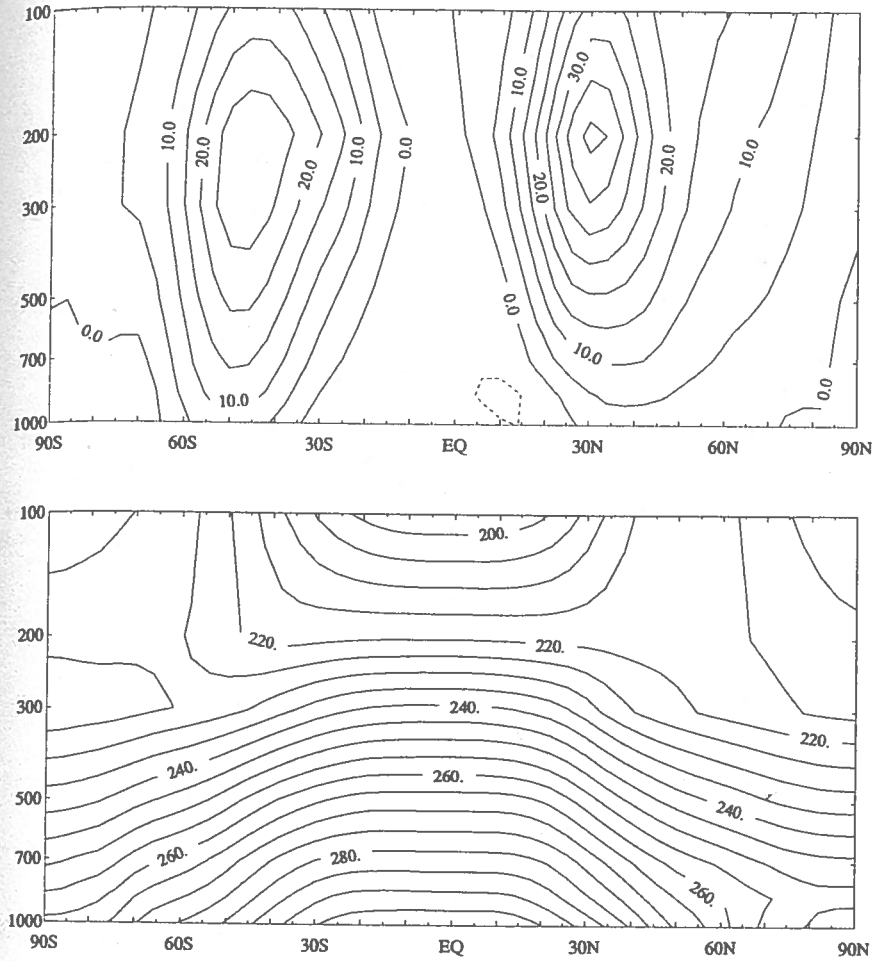

(a)

Fig. 6.1 Meridional cross sections of longitudinally averaged zonal wind (top panels, m s^{-1}) and temperature (bottom panels, contours, K) for (a) DJF and (b) JJA averaged for years 1980–1987. (Adapted from Schubert *et al.*, 1990.) (*Figure continues.*)

chapter we are concerned with the structure of the wind and temperature fields in the troposphere. The stratosphere will be discussed in Chapter 12.

The average pole-to-equator temperature gradient in the Northern Hemisphere troposphere is much larger in winter than in summer. In the Southern Hemisphere the difference between summer and winter temperature distributions is smaller, owing mainly to the large thermal inertia of the oceans

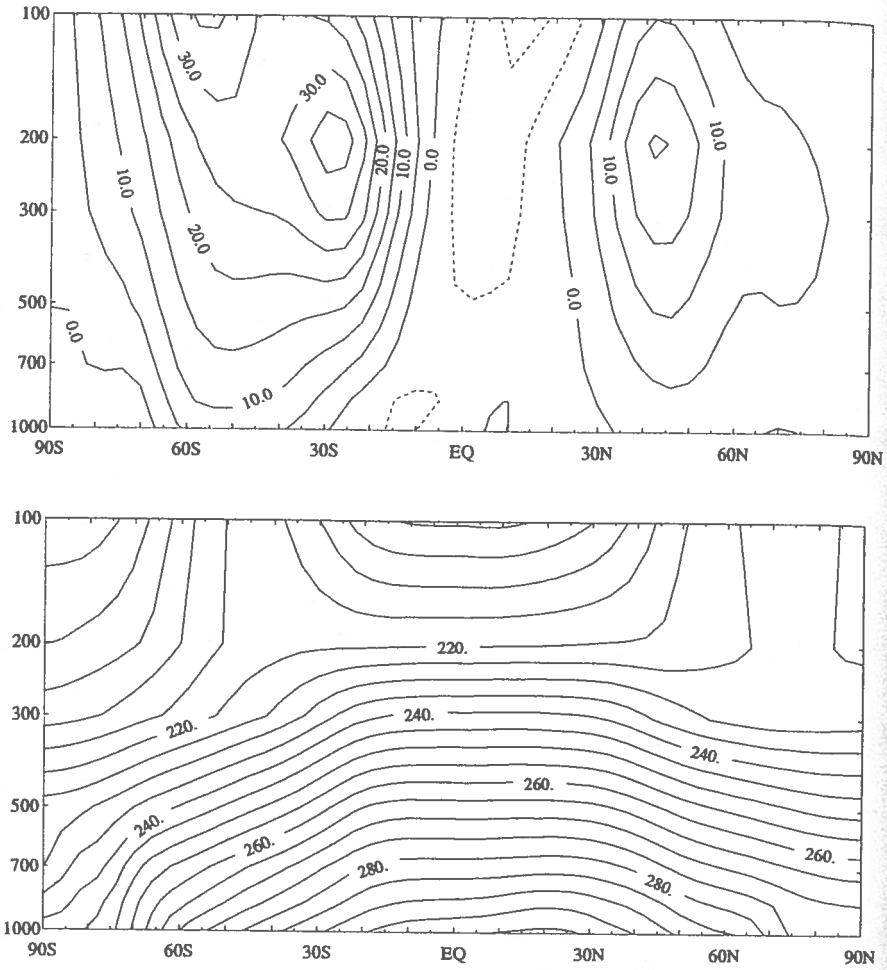

(b)

Fig. 6.1 (*Continued*)

together with the greater fraction of the surface that is covered by oceans in the Southern Hemisphere. Since the mean zonal wind and temperature fields satisfy the thermal wind relationship (3.30) to a high degree of accuracy, the maximum zonal wind speed in the Northern Hemisphere is much larger in the winter than in the summer, while there is a smaller seasonal difference in the Southern Hemisphere. Furthermore, in both seasons the core of maximum zonal wind speed (called the mean *jet stream* axis) is located just below the *tropopause* (the boundary between the troposphere and stratosphere) at the latitude where the thermal wind integrated through the troposphere is a maximum. In both hemispheres this is about 30°–35° during winter, but it moves poleward to 40°–45° during summer.

That the zonally averaged meridional cross sections of Fig. 6.1 are not representative of the mean wind structure at all longitudes can be seen in Fig. 6.2, which shows the distribution of the time-averaged zonal wind component for DJF on the 200-mb surface. It is clear from this figure that at some longitudes there are very large deviations of the time-mean zonal flow from its longitudinally averaged distribution. In particular, there are strong zonal wind maxima (jets) near 30°N just east of the Asian and Northern American continents and distinct minima in the eastern Pacific and eastern Atlantic. Synoptic-scale disturbances tend to develop preferentially in the regions of maximum time-mean zonal winds associated with the western Pacific and western Atlantic jets and to propagate downstream along *storm tracks* that approximately follow the jet axes.

The large departure of the northern winter climatological jet stream from zonal symmetry can also be readily inferred from examination of Fig. 6.3, which shows the mean 500-mb geopotential contours for January in the Northern Hemisphere. Even after averaging the height field for a month, very striking departures from zonal symmetry remain. These are clearly linked to the distributions of continents and oceans. The most prominent asymmetries are the troughs to the east of the American and Asian continents. Referring back to Fig. 6.2, we see that the intense jet at 35°N and 140°E is a result of the semipermanent trough in that region. Thus, it is

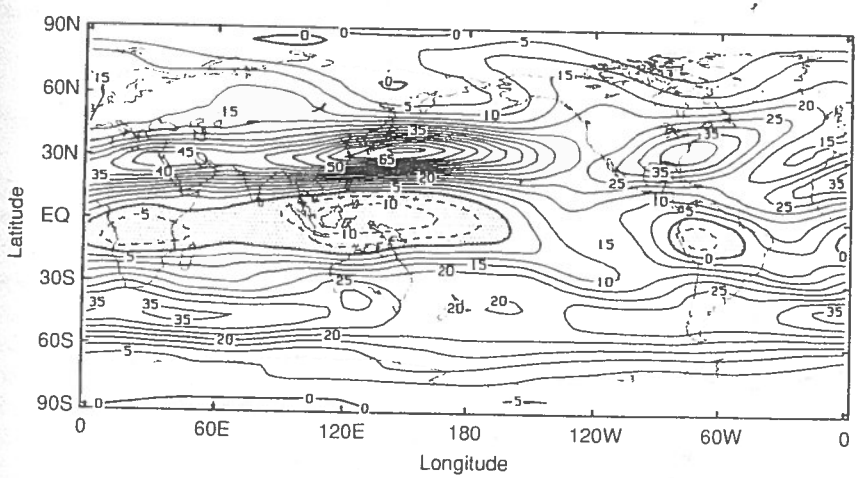

Fig. 6.2 Latitude–longitude cross section of time-averaged zonal wind speed at 200 mb for DJF averaged for years 1980–1987. (After Schubert *et al.*, 1990.)

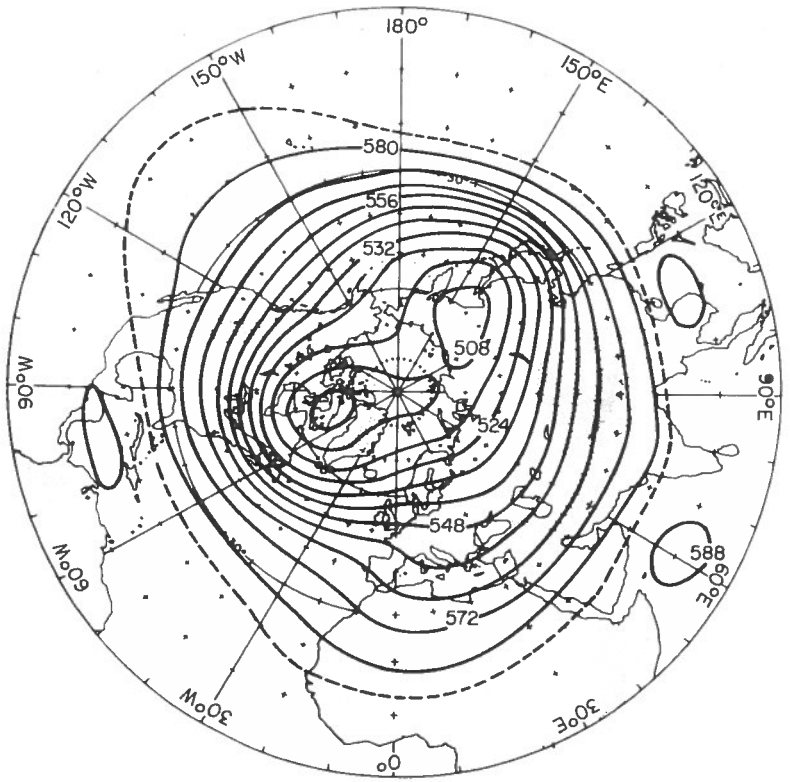

Fig. 6.3 Mean 500-mb contours in January, Northern Hemisphere. Heights shown in tens of meters. (After Palmén and Newton, 1969.)

apparent that the mean flow in which synoptic systems are embedded should really be regarded as a longitude-dependent time-averaged flow.

In addition to its longitudinal dependence, the planetary-scale flow also varies from day to day owing to its interactions with transient synoptic-scale disturbances. In fact, observations show that the transient planetary-scale flow amplitude is comparable to that of the time mean. As a result, monthly mean charts tend to smooth out the actual structure of the instantaneous jet stream since the position and intensity of the jet vary. Thus, at any time the planetary-scale flow in the region of the jet stream has much greater baroclinicity than indicated on time-averaged charts. This point is illustrated schematically in Fig. 6.4, which shows a vertical cross section through an observed jet stream over North America. Panel (a) shows the wind and temperature cross section, while panel (b) shows the wind and potential temperature. The latter provides vivid evidence of the strong static stability

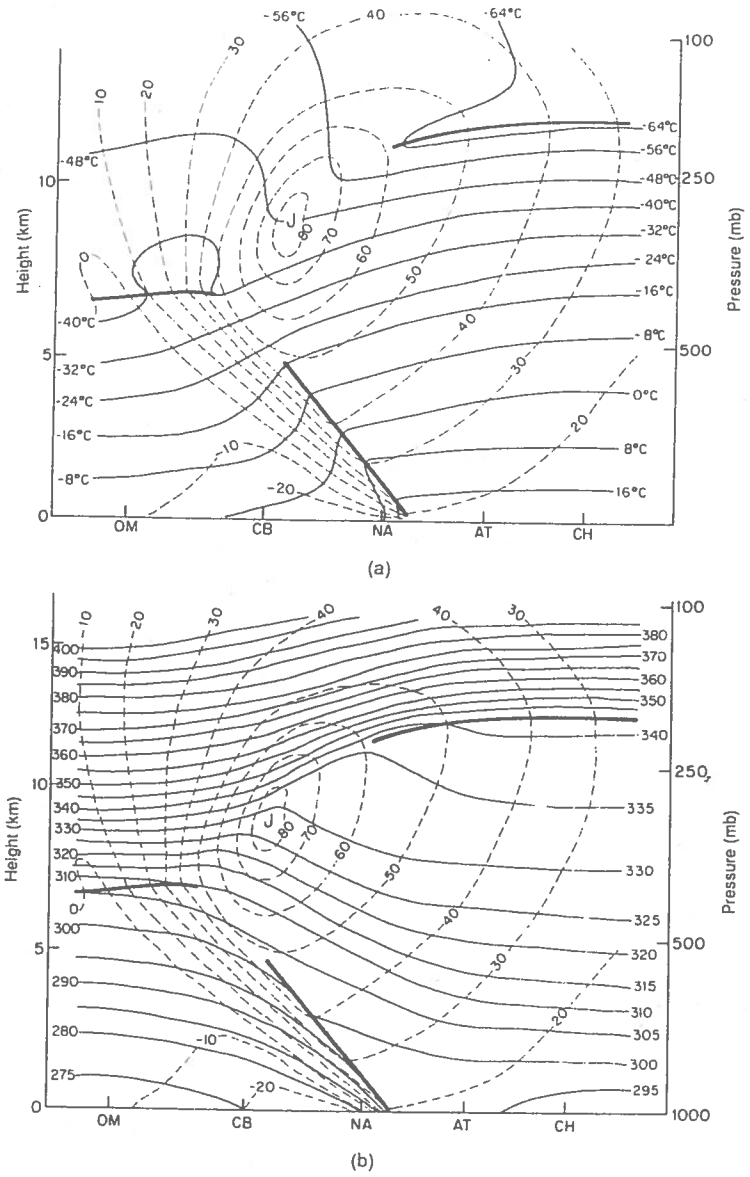

Fig. 6.4 (a) Schematic isotherms (thin solid lines, °C) and isotachs (dashed lines, m s^{-1}) in a vertical cross section through a cold front. Heavy lines mark the tropopause and frontal boundaries. The section extends approximately 1200 km in the horizontal direction. (b) Same as panel (a), but thin solid lines are potential temperature isolines in kelvins (after Wallace and Hobbs, 1977.)

in the stratosphere. It also illustrates the fact that isentropes (constant-θ surfaces) cross the tropopause in the vicinity of the jet so that adiabatic motions can exchange tropospheric and stratospheric air in that region.

At any instant the axis of the jet stream tends to be located above a narrow sloping zone of strong temperature gradients called the *polar-frontal* zone. This is the zone that in general separates the cold air of polar origin from warm tropical air. The occurrence of an intense jet core above this zone of large-magnitude temperature gradients is, of course, not mere coincidence but rather a consequence of the thermal wind balance.

It is a common observation in fluid dynamics that jets in which strong velocity shears occur may be unstable with respect to small perturbations. By this is meant that any small disturbance introduced into the jet will tend to amplify, drawing energy from the jet as it grows. Most synoptic-scale systems in midlatitudes appear to develop as the result of an instability of the jet stream flow. This instability, called *baroclinic instability*, depends on the meridional temperature gradient, particularly at the surface. Hence, through the thermal wind relationship, baroclinic instability depends on vertical shear and tends to occur in the region of the polar frontal zone.

Baroclinic instability is not, however, identical to frontal instability because most baroclinic instability models describe only geostrophically scaled motions, while disturbances in the vicinity of strong frontal zones must be highly nongeostrophic. As we shall see in Chapter 9, baroclinic disturbances may themselves act to intensify preexisting temperature gradients and hence generate frontal zones.

The stages in the development of a typical baroclinic cyclones that develops as a result of baroclinic instability are shown schematically in Fig. 6.5. In the stage of rapid development there is a cooperative interaction

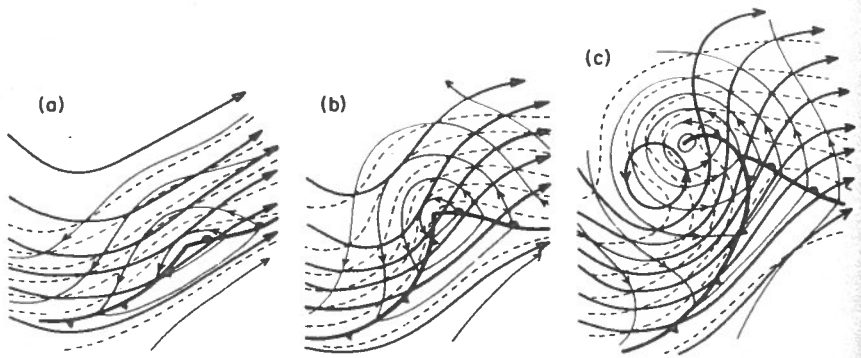

Fig. 6.5 Schematic 500-mb contours (heavy solid lines), 1000-mb contours (thin lines), and 1000–500-mb thickness (dashed) for a developing baroclinic wave at three stages of development. (After Palmén and Newton, 1969.)

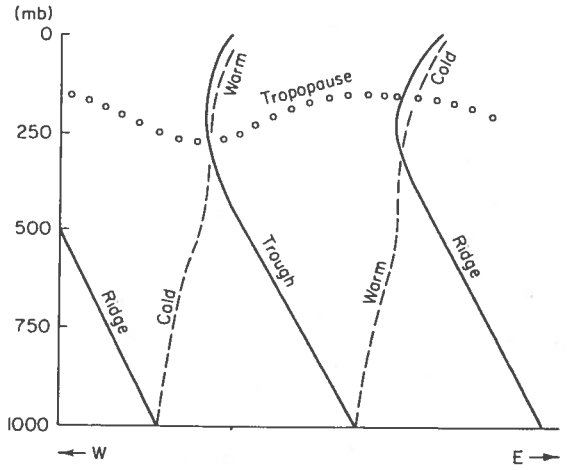

Fig. 6.6 West–east cross section through developing baroclinic wave. Solid lines are trough and ridge axes; dashed lines are axes of temperature extrema; the chain of open circles denotes the tropopause.

between the upper level and surface flows; strong cold advection is seen to occur west of the trough at the surface, with weaker warm advection to the east. This pattern of thermal advection is a direct consequence of the fact that the trough at 500 mb lags (lies to the west of) the surface trough so that the mean geostrophic wind in the 1000–500-mb layer is directed across the 1000–500-mb thickness lines toward larger thickness west of the surface trough and toward smaller thickness east of the surface trough. This dependence of the phase of the disturbance on height is better illustrated by Fig. 6.6, which shows a schematic downstream (or west–east) cross section through an idealized developing baroclinic system. Throughout the troposphere the trough and ridge axes tilt westward (or upstream) with height,[1] while the axes of warmest and coldest air are observed to have the opposite tilt. As we shall see later the westward tilt of the troughs and ridges is necessary in order that the mean flow give up potential energy to the developing wave. In the mature stage (not shown in Fig. 6.5) the troughs at 500 and 1000 mb are nearly in phase. As a consequence, the thermal advection and energy conversion are quite weak.

6.2 The Quasi-geostrophic Approximation

The main goal of this chapter is to show how the observed structure of midlatitude synoptic systems can be interpreted in terms of the constraints

[1] In reality the phase tilts tend to be concentrated below the 700-mb level.

imposed on synoptic-scale motions by the dynamical equations. Specifically we show that for motions that are hydrostatic and nearly geostrophic, the three-dimensional flow field is determined approximately by the isobaric distribution of geopotential [$\Phi(x, y, p, t)$]. For this analysis, it is convenient to use the isobaric coordinate system both because meteorological measurements are generally referred to constant-pressure surfaces and because the dynamical equations are somewhat simpler in isobaric coordinates than in height coordinates. Thus, use of the isobaric coordinate system simplifies the development of approximate prognostic and diagnostic equations.

6.2.1 Scale Analysis in Isobaric Coordinates

The dynamical equations in isobaric coordinates were developed in Section 3.1 and for reference are repeated here. The horizontal momentum equation, the hydrostatic equation, the continuity equation, and the thermodynamic energy equation may be expressed as follows:

$$\frac{D\mathbf{V}}{Dt}+f\mathbf{k}\times\mathbf{V}=-\nabla\Phi \tag{6.1}$$

$$\frac{\partial\Phi}{\partial p}=-\alpha=-\frac{RT}{p} \tag{6.2}$$

$$\nabla\cdot\mathbf{V}+\frac{\partial\omega}{\partial p}=0 \tag{6.3}$$

$$\left(\frac{\partial}{\partial t}+\mathbf{V}\cdot\nabla\right)T-S_p\omega=\frac{J}{c_p} \tag{6.4}$$

Here the total derivative in (6.1) is defined by

$$\frac{D}{Dt}\equiv\left(\frac{\partial}{\partial t}\right)_p+(\mathbf{V}\cdot\nabla)_p+\omega\frac{\partial}{\partial p} \tag{6.5}$$

where $\omega\equiv Dp/Dt$ is the individual pressure change, and in (6.4) $S_p\equiv -T\,\partial\ln\theta/\partial p$ is the static stability parameter [$S_p\approx 5\times10^{-4}\ \mathrm{K\ Pa^{-1}}$ in the midtroposphere].

These equations, although simplified by use of the hydrostatic approximation and by neglect of some small terms that appear in the complete spherical coordinate form, still contain several terms that are of secondary significance for midlatitude synoptic-scale systems. They can be further simplified by recalling from Section 2.4 that the horizontal flow is nearly geostrophic and that the magnitude of the ratio of vertical velocity to horizontal velocity is of order 10^{-3}.

We first separate the horizontal velocity into geostrophic and ageostrophic parts by letting

$$\mathbf{V}=\mathbf{V}_g+\mathbf{V}_a \tag{6.6}$$

where the geostrophic wind is defined as

$$\mathbf{V}_g\equiv f_0^{-1}\mathbf{k}\times\nabla\Phi \tag{6.7}$$

and $\mathbf{V}_a$ is just the difference between the total horizontal wind and the geostrophic wind. Here we have assumed that the meridional length scale, L, is small compared to the radius of the earth so that the geostrophic wind (6.7) may be defined using a constant reference latitude value of the Coriolis parameter.[2]

For the systems of interest $|\mathbf{V}_g|\gg|\mathbf{V}_a|$. More precisely,

$$|\mathbf{V}_a|/|\mathbf{V}_g|\sim O(\mathrm{Ro})$$

That is, the ratio of the magnitudes of the ageostrophic and geostrophic winds is the same order of magnitude as the Rossby number introduced in Section 2.4.2.

The momentum can then be approximated to $O(\mathrm{Ro})$ by its geostrophic value, and the rate of change of momentum or temperature following the horizontal motion can be approximated to the same order by the rate of change following the geostrophic wind. Thus, in (6.5) $\mathbf{V}$ can be replaced by $\mathbf{V}_g$ and the vertical advection, which arises only from the ageostrophic flow, can be neglected. The rate of change of momentum following the total motion is then approximately equal to the rate of change of the geostrophic momentum following the geostrophic wind:

$$\frac{D\mathbf{V}}{Dt}\approx\frac{D_g\mathbf{V}_g}{Dt}$$

where

$$\frac{D_g}{Dt}\equiv\frac{\partial}{\partial t}+\mathbf{V}_g\cdot\nabla=\frac{\partial}{\partial t}+u_g\frac{\partial}{\partial x}+v_g\frac{\partial}{\partial y} \tag{6.8}$$

[2] This definition of the geostrophic wind will be referred to as *constant-f* (CF) geostrophy, while the definition given in (3.4) will be called *variable-f* (VF) geostrophy. The CF geostrophic wind is nondivergent, while the VF geostrophic wind has a divergent portion (see Problem 3.19). The interpretation of the ageostrophic wind depends strongly on which type of geostrophy is used, as explained in Blackburn (1985).

Although a constant f_0 can be used in defining $\mathbf{V}_g$, it is still necessary to retain the dynamical effect of the variation of the Coriolis parameter with latitude in the Coriolis force term in the momentum equation. This variation can be approximated by expanding the latitudinal dependence of f in a Taylor series about a reference latitude ϕ_0 and retaining only the first two terms to yield

$$f = f_0 + \beta y \tag{6.9}$$

where $\beta \equiv (df/dy)_{\phi_0} = 2\Omega \cos \phi_0 / a$ and $y = 0$ at ϕ_0. This approximation is usually referred to as the *midlatitude beta-plane* approximation. For synoptic-scale motions the ratio of the first two terms in the expansion of f has order of magnitude

$$\frac{\beta L}{f_0} \sim \frac{\cos \phi_0}{\sin \phi_0} \frac{L}{a} \sim O(\mathrm{Ro}) \ll 1$$

This justifies letting the Coriolis parameter have a constant value f_0 in the geostrophic approximation and approximating its variation in the Coriolis force term by (6.9).

From (6.1) the acceleration following the motion is equal to the difference between the Coriolis force and the pressure gradient force. This difference depends on the departure of the actual wind from the geostrophic wind. Thus, it is not permissible simply to replace the horizontal velocity by its geostrophic value in the Coriolis term. Rather, we use (6.6), (6.7), and (6.9) to write

$$\begin{aligned} f\mathbf{k} \times \mathbf{V} + \nabla\Phi &= (f_0 + \beta y)\mathbf{k} \times (\mathbf{V}_g + \mathbf{V}_a) - f_0 \mathbf{k} \times \mathbf{V}_g \\ &\approx f_0 \mathbf{k} \times \mathbf{V}_a + \beta y \mathbf{k} \times \mathbf{V}_g \end{aligned} \tag{6.10}$$

where we have used the geostrophic relation (6.7) to eliminate the pressure gradient force and neglected the ageostrophic wind compared to the geostrophic wind in the term proportional to βy. The approximate horizontal momentum equation thus has the form

$$\frac{D_g \mathbf{V}_g}{Dt} = -f_0 \mathbf{k} \times \mathbf{V}_a - \beta y \mathbf{k} \times \mathbf{V}_g \tag{6.11}$$

Each term in (6.11) is thus $O(\mathrm{Ro})$ compared to the pressure gradient force, while terms neglected are $O(\mathrm{Ro}^2)$ or smaller.

The geostrophic wind defined in (6.7) is nondivergent. Thus,

$$\nabla \cdot \mathbf{V} = \nabla \cdot \mathbf{V}_a = \frac{\partial u_a}{\partial x} + \frac{\partial v_a}{\partial y}$$

and the continuity equation (6.3) can be rewritten as

$$\nabla \cdot \mathbf{V}_a + \frac{\partial \omega}{\partial p} = 0 \tag{6.12}$$

which shows that if the geostrophic wind is defined by (6.7), ω is determined only by the ageostrophic part of the wind field.

In the thermodynamic energy equation (6.4) the horizontal advection can be approximated by its geostrophic value. However, the vertical advection is not neglected but forms part of the adiabatic heating and cooling term. This term must be retained because the static stability is usually large enough on the synoptic scale that the adiabatic heating or cooling owing to vertical motion is of the same order as the horizontal temperature advection despite the smallness of the vertical velocity. It can be somewhat simplified, though, by dividing the total temperature field, T_{tot}, into a basic state (standard atmosphere) portion that depends only on pressure, $T_0(p)$, plus a deviation from the basic state, $T(x, y, p, t)$, as was done for potential temperature in Section 2.7.4. Thus we let

$$T_{\mathrm{tot}}(x, y, p, t) = T_0(p) + T(x, y, p, t)$$

Now since $|dT_0/dp| \gg |\partial T/\partial p|$ only the basic state portion of the temperature field need be included in the static stability term and the quasi-geostrophic thermodynamic energy equation may be expressed in the form

$$\left(\frac{\partial}{\partial t} + \mathbf{V}_g \cdot \nabla\right) T - \left(\frac{\sigma p}{R}\right) \omega = \frac{J}{c_p} \tag{6.13}$$

where $\sigma \equiv -RT_0 p^{-1}\, d \ln \theta_0/dp$ and θ_0 is the potential temperature corresponding to the basic state temperature T_0 ($\sigma \approx 2 \times 10^{-6}\ \mathrm{m^2\ Pa^{-2}\ s^{-2}}$ in the midtroposphere).

Equations (6.2), (6.7), (6.11), (6.12), and (6.13) constitute the quasi-geostrophic equations. If J is known these form a complete set in the dependent variables Φ, T, $\mathbf{V}_g$, $\mathbf{V}_a$, and ω. This form is particularly useful when information is needed on the distribution of the ageostrophic velocity. However, when $\mathbf{V}_a$ is not required it may be eliminated to produce a somewhat simpler set.

6.2.2 The Quasi-geostrophic Vorticity Equation

Just as the horizontal momentum can be approximated to $O(\mathrm{Ro})$ by its geostrophic value, the vertical component of vorticity can also be approximated geostrophically. If the CF geostrophic relationship (6.7) is expanded in Cartesian coordinates as

$$f_0 v_g = \frac{\partial \Phi}{\partial x}, \qquad f_0 u_g = -\frac{\partial \Phi}{\partial y} \tag{6.14}$$

the geostrophic vorticity, $\zeta_g = \mathbf{k} \cdot \nabla \times \mathbf{V}_g$, can be expressed in terms of the horizontal Laplacian of the geopotential:

$$\zeta_g = \frac{\partial v_g}{\partial x} - \frac{\partial u_g}{\partial y} = \frac{1}{f_0}\left(\frac{\partial^2 \Phi}{\partial x^2} + \frac{\partial^2 \Phi}{\partial y^2}\right) = \frac{1}{f_0}\nabla^2 \Phi \tag{6.15}$$

Equation (6.15) can be used to determine $\zeta_g(x, y)$ from a known field $\Phi(x, y)$. Alternatively, (6.15) can be solved by inverting the Laplacian operator to determine Φ from a known distribution of ζ_g provided that suitable conditions on Φ are specified on the boundaries of the region in question. This *invertibility* is one reason why vorticity is such a useful forecast diagnostic; if the evolution of the vorticity can be predicted, then inversion of (6.15) yields the evolution of the geopotential field, from which it is possible to determine the geostrophic wind. Since the Laplacian of a function tends to be a maximum where the function itself is a minimum, positive vorticity implies low values of geopotential and vice versa, as illustrated for a simple sinusoidal disturbance in Fig. 6.7.

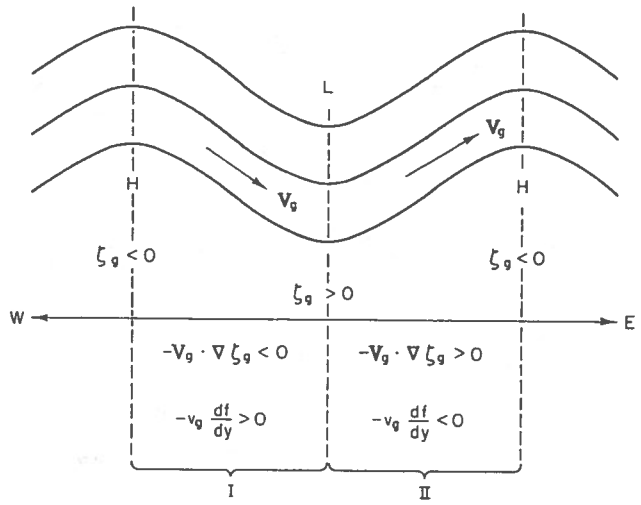

Fig. 6.7 Schematic 500-mb geopotential field showing regions of positive and negative advections of relative and planetary vorticity.

The quasi-geostrophic vorticity equation can be obtained from the x and y components of the quasi-geostrophic momentum equation (6.11), which can be expressed respectively as

$$\frac{D_g u_g}{Dt} - f_0 v_a - \beta y v_g = 0 \tag{6.16}$$

and

$$\frac{D_g v_g}{Dt} + f_0 u_a + \beta y u_g = 0 \tag{6.17}$$

Taking $\partial(6.17)/\partial x - \partial(6.16)/\partial y$ and using the fact that the divergence of the CF geostrophic wind vanishes immediately yields the vorticity equation

$$\frac{D_g \zeta_g}{Dt} = -f_0\left(\frac{\partial u_a}{\partial x} + \frac{\partial v_a}{\partial y}\right) - \beta v_g \tag{6.18}$$

which should be compared with (4.22).

Noting that since f depends only on y so that $D_g f / Dt = \mathbf{V}_g \cdot \nabla f = \beta v_g$ and that the divergence of the ageostrophic wind can be eliminated in favor of ω using (6.12), we can rewrite (6.18) as

$$\frac{\partial \zeta_g}{\partial t} = -\mathbf{V}_g \cdot \nabla(\zeta_g + f) + f_0 \frac{\partial \omega}{\partial p} \tag{6.19}$$

which states that the local rate of change of geostrophic vorticity is given by the sum of the advection of the absolute vorticity by the geostrophic wind plus the concentration or dilution of vorticity by stretching or shrinking of fluid columns (the divergence effect).

The vorticity tendency owing to vorticity advection [the first term on the right in (6.19)] may be rewritten as

$$-\mathbf{V}_g \cdot \nabla(\zeta_g + f) = -\mathbf{V}_g \cdot \nabla \zeta_g - \beta v_g$$

The two terms on the right represent the geostrophic advections of relative vorticity and planetary vorticity, respectively. For disturbances in the westerlies, these two effects tend to have opposite signs as illustrated schematically in Fig. 6.7 for an idealized 500-mb flow.

In region I upstream of the 500-mb trough, the geostrophic wind is directed from the negative vorticity maximum at the ridge toward the positive vorticity maximum at the trough so that $-\mathbf{V}_g \cdot \nabla \zeta_g < 0$. But at the same time, since $v_g < 0$ in region I, the geostrophic wind has its y component directed down the gradient of planetary vorticity so that $-\beta v_g > 0$. Hence, in region I the advection of relative vorticity tends to decrease the local vorticity, whereas advection of planetary vorticity tends to increase the local vorticity. Similar arguments (but with reversed signs) apply to region II. Therefore, advection of relative vorticity tends to move the vorticity pattern and hence the troughs and ridges eastward (downstream). But advection of planetary vorticity tends to move the troughs and ridges westward against the advecting wind field. The latter motion is called *retrograde* motion or *retrogression.*

The net effect of advection on the evolution of the vorticity pattern depends upon which type of vorticity advection dominates. In order to compare the magnitudes of the relative and planetary vorticity advections, we assume that Φ on the midlatitude β plane can be represented as the sum of a time and zonally averaged part, which depends on y and p, and a fluctuating part that has a sinusoidal dependence in x, and y:

$$\Phi(x, y, p, t) = \bar{\Phi}(y, p) + \Phi'(p, t) \sin kx \cos ly$$

where Φ' is the amplitude of the fluctuating component and the *wave numbers* k and l are defined as $k = 2\pi/L_x$ and $l = 2\pi/L_y$ with L_x and L_y the wavelengths in the x and y directions, respectively. We further assume that

$$\bar{\Phi}(y, p) = \Phi_0(p) - f_0 U y$$

where Φ_0 is a standard atmosphere geopotential distribution and U is a constant mean zonal wind. The geostrophic vorticity is then simply

$$\begin{aligned} \zeta_g = f_0^{-1} \nabla^2 \Phi &= -f_0^{-1}(k^2 + l^2)\Phi' \sin kx \cos ly \\ &= -f_0^{-1}(k^2 + l^2)(\Phi - \bar{\Phi}) \end{aligned} \tag{6.20}$$

The patterns of geopotential and relative vorticity for this case are shown in Fig. 6.8. For a disturbance with a given amplitude of geopotential disturbance, Φ', the amplitude of the vorticity increases as the square of the wave number or inversely as the square of the horizontal scale. As a consequence, the advection of relative vorticity dominates over planetary vorticity advection for short waves ($L_x < 3000$ km), while for long waves

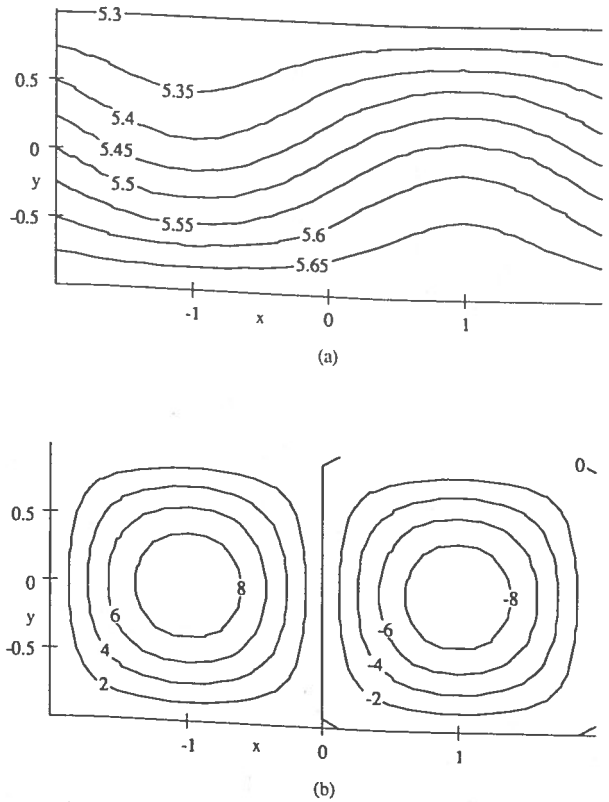

Fig. 6.8 Geopotential in units of $10^4\ m^2\ s^{-2}$ (a) and relative vorticity in units of $10^{-6}\ s^{-1}$ (b) for the sinusoidal disturbance of Eq. (6.20). Here $\Phi_0 = 5 \times 10^4\ m^2\ s^{-2}$, $f_0 = 10^{-4}\ s^{-1}$, $\Phi' = 800\ m^2\ s^{-2}$, $U = 10\ m\ s^{-1}$, and $k = l = (\pi/2) \times 10^{-6}\ m^{-1}$. Axes are labeled in units of 10^3 km.

($L_x > 10{,}000$ km) the planetary vorticity advection tends to dominate. Therefore, as a general rule short-wavelength synoptic-scale systems should move eastward with the advecting zonal flow while long planetary waves should tend to retrogress (move westward against the mean flow).[3] Waves of intermediate wavelength may be quasi-stationary or move eastward much slower than the mean geostrophic wind speed. Since positive maxima in relative vorticity are associated with cyclonic disturbances, regions of positive vorticity advection, which can easily be estimated from upper-level

[3] Observed long waves tend to remain stationary rather than to retrogress. This is believed to be a result of processes such as nonlinear interactions with transient short waves, forcing owing to topographic influences, and diabatic heating contrasts associated with land-sea differences, as was mentioned in Section 6.1.

maps, are commonly used as aids in forecasting synoptic-scale weather disturbances.

Vorticity advection does not alone determine the evolution of meteorological systems. A change in the vertical shear of the horizontal wind associated with differential (i.e., height-dependent) vorticity advection will drive an ageostrophic vertical circulation, which adiabatically adjusts the horizontal temperature gradient to maintain thermal wind balance. The convergence and divergence fields associated with this vertical circulation will not only modify the effects of vorticity advection at upper levels but also force changes in the vorticity distribution in the lower troposphere, where advection may be very weak.

In an analogous manner, thermal advection, which is often strong near the surface, does not merely force changes in the temperature in the lower troposphere. Rather, it induces a vertical circulation, which through its associated divergence and convergence patterns alters the vorticity fields both near the surface and aloft so that thermal wind balance is maintained.

The vertical circulation induced by quasi-geostrophic differential vorticity advection and thermal advection is generally an order of magnitude larger than that induced by boundary layer pumping (5.38). Thus, it is reasonable to neglect boundary layer effects to a first approximation in quasi-geostrophic theory.

6.3 Quasi-geostrophic Prediction

The characteristics of the geostrophic circulation forced by the vertical motions associated with vorticity and thermal advection can be determined without explicitly determining the distribution of ω. Since T, ζ_g, and $\mathbf{V}_g$ are all functions of Φ, the quasi-geostrophic vorticity equation (6.19) and the thermodynamic energy equation (6.13) each can be written so that they contain only the two dependent variables Φ and ω. (For simplicity we ignore the diabatic heating term in the thermodynamic energy equation even though it may be important in some synoptic disturbances.) It is thus possible to eliminate ω between these two equations and obtain an equation relating Φ to $\partial\Phi/\partial t$. Defining the geopotential tendency $\chi \equiv \partial\Phi/\partial t$, using the hydrostatic equation (6.2) to eliminate T in favor of $\partial\Phi/\partial p$, and recalling that the order of partial differentiation may be reversed without changing the result, the thermodynamic energy equation (6.13) and the geostrophic vorticity equation (6.19) can be expressed respectively as

$$\frac{\partial \chi}{\partial p} = -\mathbf{V}_g \cdot \nabla\left(\frac{\partial \Phi}{\partial p}\right) - \sigma\omega \tag{6.21}$$

and

$$\nabla^2 \chi = -f_0 \mathbf{V}_g \cdot \nabla\left(\frac{1}{f_0}\nabla^2\Phi + f\right) + f_0^2 \frac{\partial \omega}{\partial p} \tag{6.22}$$

where σ was defined below (6.13) and we have used (6.15) to write the geostrophic vorticity and its tendency in terms of the Laplacian of geopotential.

Equations (6.21) and (6.22) are one form of the *quasi-geostrophic system.* The first of these indicates that the vertical derivative of the geopotential tendency is equal to the sum of thickness advection and adiabatic thickness change owing to vertical motion. The second indicates that the horizontal Laplacian of the geopotential tendency is equal to the sum of vorticity advection plus vorticity generation by the divergence effect. Purely geostrophic motion ($\omega = 0$) is a solution to (6.21)-(6.22) only in very special situations such as barotropic flow (no pressure dependence) or zonally symmetric flow (no x dependence). More general purely geostrophic flows cannot satisfy both these equations simultaneously, since there are then two independent equations in a single unknown, so that the system is overdetermined. Thus, it should be clear that the role of the vertical motion distribution must be to maintain consistency between the geopotential tendencies required by thermal advection in (6.21) and vorticity advection in (6.22), respectively.

6.3.1 Geopotential Tendency

If we multiply (6.21) by f_0^2/σ and then differentiate with respect to pressure and add the result to (6.22), ω is eliminated and we obtain an equation that determines the local rate of change of geopotential in terms of the three-dimensional distribution of the Φ field:

$$\underbrace{\left[\nabla^2 + \frac{\partial}{\partial p}\left(\frac{f_0^2}{\sigma}\frac{\partial}{\partial p}\right)\right]}_{\text{A}}\chi = \underbrace{-f_0 \mathbf{V}_g \cdot \nabla\left(\frac{1}{f_0}\nabla^2\Phi + f\right)}_{\text{B}} \underbrace{-\frac{\partial}{\partial p}\left[-\frac{f_0^2}{\sigma}\mathbf{V}_g \cdot \nabla\left(-\frac{\partial \Phi}{\partial p}\right)\right]}_{\text{C}} \tag{6.23}$$

This equation is often referred to as the *geopotential tendency equation.* It provides a relationship between the local change of geopotential and the

distributions of vorticity and thickness advection as can be seen by analyzing the three terms labeled A, B, and C, respectively. If the distribution of Φ is known at a given time, terms B and C may be regarded as known forcing functions, and (6.23) is a linear partial differential equation in the unknown χ.

Although (6.23) appears to be quite complicated, a qualitative notion of its implications can be gained by examining the solution for a simple wave pattern. Term A in (6.23) involves only second derivatives in space of the χ field. We showed in (6.20) that for wavelike disturbances the horizontal Laplacian of Φ is proportional to the negative of the deviation of Φ from its mean. A similar relationship holds for χ. Thus, letting

$$\chi(x, y, p, t) \approx X(p, t) \sin kx \cos ly$$

we have $\nabla^2\chi \approx -(k^2+l^2)\chi$. The forcing terms B and C in (6.23) are also assumed to have sinusoidal behavior in x and y:

$$-f_0 \mathbf{V}_g \cdot \boldsymbol{\nabla}\left(\frac{1}{f_0}\nabla^2\Phi + f\right) \approx F_v(p) \sin kx \cos ly$$

$$-\frac{f_0^2}{\sigma}\mathbf{V}_g \cdot \boldsymbol{\nabla}\left(-\frac{\partial\Phi}{\partial p}\right) \approx F_T(p) \sin kx \cos ly$$

where $F_v(p)$ and $F_T(p)$ represent the vertical dependences of the vorticity advection and thermal advection, respectively. Substituting these expressions into (6.23) and eliminating the sin kx cos ly dependence, which is common to each term, we obtain an ordinary differential equation for the vertical dependence of the geopotential tendency:

$$\frac{d^2X}{dp^2} - \lambda^2 X = \frac{\sigma}{f_0^2}\left(F_v - \frac{dF_T}{dp}\right) \tag{6.24}$$

where $\lambda^2 \equiv (k^2+l^2)\sigma f_0^{-2}$ and we have neglected the pressure dependence of static stability.[4] Equation (6.24) shows that forcing at a given altitude will

[4] Actually, σ varies substantially with pressure even in the troposphere. However, the qualitative discussion in this section would not be changed if we were to include this additional complication.

generate a response whose vertical scale (measured in pressure units) is λ^{-1}. Thus, for example, upper-level vorticity advection associated with disturbances of large horizontal scale (small k and l) will produce geopotential tendencies that extend down to the surface with little loss of amplitude, while for disturbances of small horizontal scale the response is confined close to the levels of forcing (see Fig. 6.9). In mathematical terms, the differential operator in (6.24) spreads the response in the vertical so that forcing at one altitude influences other altitudes.

The role of thermal advection in changing upper-level geopotential heights can be simply illustrated by considering the special case of $\beta = 0$ and very large horizontal scale so that $\lambda^2 \to 0$ and $F_v \approx 0$. Eq. (6.24) can then be approximated as

$$d^2X/dp^2 \approx -\sigma f_0^{-2}(dF_T/dp)$$

Using the definitions of X and F_T and integrating twice with respect to pressure yields

$$X(p) - X(p_0) \approx -\frac{\sigma}{f_0^2}\int_{p_0}^{p} F_T\, dp$$

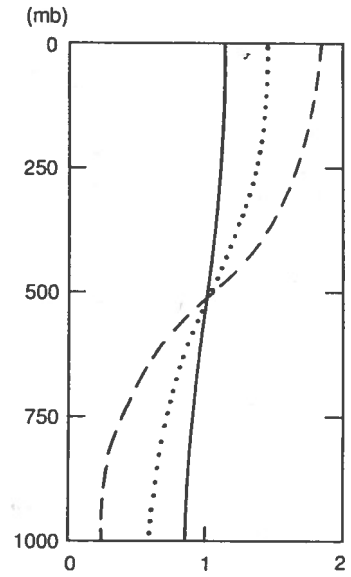

Fig. 6.9 Vertical structure of the geopotential tendency (units of $10^{-2}\,m^2\,s^{-3}$) owing to forcing by vorticity advection. Here, $l=0$, $k=2\pi/L_x$, $F_v = 2\times10^{-2}\,k^2\,s^{-3}$, for $p<500$ mb and $F_v=0$ for $p>500$ mb, $\lambda^2 = 200\,k^2$ $Pa^{-2}\,m^{-2}$, and $L_x = 2{,}000$ km (dashed line), $L_x = 4{,}000$ km (dotted line), and $L_x = 8{,}000$ km (solid line).

After multiplying both sides by sin kx cos ly and using the definitions of X and F_T, this may be rewritten as

$$\frac{\partial}{\partial t}[\Phi(p)-\Phi(p_0)]=\frac{\partial}{\partial t}\delta\Phi\approx -R\int_p^{p_0}\mathbf{V}_g\cdot\nabla T\,d\ln p$$

which states that the thickness tendency for the column between pressure levels p_0 and p is proportional to the vertically integrated temperature advection.

Term B in (6.23), the vorticity advection term, generally is the main forcing term in the upper troposphere. As the discussion in the previous subsection indicated, for short waves term B is negative in region I (upstream of the 500-mb trough.) Thus, since the sign of the geopotential tendency is opposite to that of the forcing in this case, χ will be positive and a ridge will tend to develop. This ridging is, of course, necessary for the development of a negative geostrophic vorticity. Similar arguments, but with the signs reversed, apply to region II downstream from the 500-mb trough, where falling geopotential heights are associated with a positive relative vorticity advection. It is also important to note that the vorticity advection term is zero along both the trough and ridge axes since both $\nabla\zeta_g$ and v_g are zero at the axes. Thus, vorticity advection cannot change the strength of this type of disturbance at the levels where the advection is occurring but only acts to propagate the disturbance horizontally and spread it vertically.

The major mechanism for amplification or decay of midlatitude synoptic systems is contained in term C of (6.23). This term involves the rate of change with pressure of the horizontal thickness advection. (If we had retained the diabatic heating term it would have contributed in a similar fashion.) The thickness advection tends to be largest in magnitude in the lower troposphere beneath the 500-mb trough and ridge lines in a developing baroclinic wave. Now since $-\partial\Phi/\partial p$ is proportional to temperature, the thickness advection is proportional to the temperature advection. Thus, term C in (6.23) is proportional to minus the rate of change of temperature advection with respect to pressure (i.e., plus the rate of change with respect to height). This term is sometimes referred to as the *differential temperature advection.*

To examine the influence of differential temperature advection on the geopotential tendency we consider the idealized developing wave shown in Fig. 6.5. Below the 500-mb ridge there is strong warm advection associated with the warm front, while below the 500-mb trough there is strong cold advection associated with the cold front. Above the 500-mb level the temperature gradient is usually weaker, and the isotherms often become nearly parallel to the height lines, so that thermal advection tends to be small.

Thus, in contrast to term B in (6.23), the forcing term C is concentrated in the lower troposphere. But again, the geopotential tendency response is not limited to the levels of forcing but is spread in the vertical, so that for developing waves it will deepen upper-level troughs and build upper-level ridges.

In the region of warm advection $-\mathbf{V}_g\cdot\nabla(-\partial\Phi/\partial p)>0$ since $\mathbf{V}_g$ has a component down the temperature gradient. But, as explained above, the warm advection decreases with height (increases with pressure) so that $\partial[-\mathbf{V}_g\cdot\nabla(-\partial\Phi/\partial p)]/\partial p>0$. Conversely, beneath the 500-mb trough where there is cold advection decreasing with height, the opposite signs obtain. Therefore, along the 500-mb trough and ridge axes where the vorticity advection is zero the tendency equation states that for a developing wave

$$\chi\sim\begin{cases}\dfrac{\partial}{\partial p}\left[-\mathbf{V}_g\cdot\nabla\left(-\dfrac{\partial\Phi}{\partial p}\right)\right]>0 & \text{at the ridge}\\ <0 & \text{at the trough}\end{cases}$$

Therefore, as indicated in Fig. 6.10, the effect of cold advection below the 500-mb trough is to *deepen* the trough in the upper troposphere, and the effect of warm advection below the 500-mb ridge is to *build* the ridge in

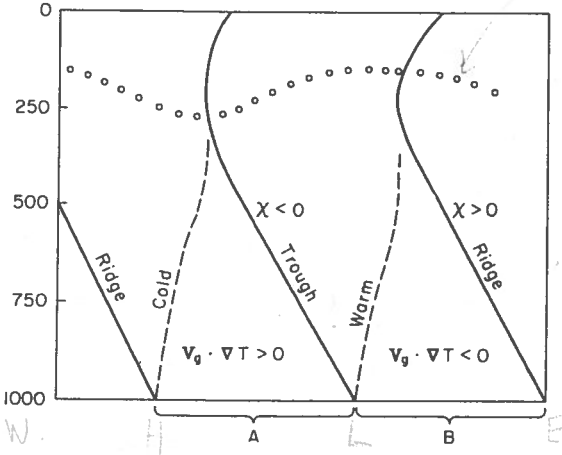

Fig. 6.10 East–west section through a developing synoptic disturbance showing the relationship of temperature advection to the upper-level height tendencies. A and B designate, respectively, regions of cold advection and warm advection in the lower troposphere.

the upper troposphere. Hence, differential temperature or thickness advection, even if limited to the lower troposphere, intensifies the upper-level troughs and ridges in a developing system.

Qualitatively, the effects of differential temperature advection are easily understood since the advection of cold air into the air column below the 500-mb trough reduces the thickness of that column and hence lowers the height of the 500-mb surface unless there is a compensating rise in the surface pressure. Obviously, warm advection into the air column below the ridge has the opposite effect.

In summary, we have shown that in the absence of diabatic heating the horizontal temperature advection must be nonzero in order that a mid-latitude synoptic system intensify through baroclinic processes. As we shall see in Chapter 8, the temperature advection pattern described above indirectly implies conversion of potential energy to kinetic energy.

6.3.2 The Quasi-geostrophic Potential Vorticity Equation

The geopotential tendency equation stated in the form (6.23) is useful for physical motivation of processes leading to geopotential changes (and hence upper-level troughing and ridging) since the tendency χ is related to the easily comprehended processes of vorticity and temperature advection. However, this form of the equation actually conceals its true character as a conservation equation for a field commonly referred to as *quasi-geostrophic potential vorticity*. To put (6.23) in conservation form, we again neglect the diabatic heating term and simplify the right-hand side by using the chain rule of differentiation to write term C as

$$-\left(\mathbf{V}_g \cdot \nabla \frac{\partial}{\partial p}\left(\frac{f_0^2}{\sigma}\frac{\partial \Phi}{\partial p}\right) + \frac{f_0^2}{\sigma}\frac{\partial \mathbf{V}_g}{\partial p} \cdot \nabla \frac{\partial \Phi}{\partial p}\right)$$

But $f_0\, \partial \mathbf{V}_g/\partial p = \mathbf{k} \times \nabla(\partial \Phi/\partial p)$, which is perpendicular to $\nabla(\partial \Phi/\partial p)$. Thus, the second part of the above expression vanishes and the first part can be combined with term B in (6.23) to yield

$$\left(\frac{\partial}{\partial t} + \mathbf{V}_g \cdot \nabla\right)\left[\frac{1}{f_0}\nabla^2 \Phi + f + \frac{\partial}{\partial p}\left(\frac{f_0}{\sigma}\frac{\partial \Phi}{\partial p}\right)\right] = \frac{D_g q}{Dt} = 0 \tag{6.25}$$

where q is the quasi-geostrophic potential vorticity defined by

$$q \equiv \left[\frac{1}{f_0}\nabla^2 \Phi + f + \frac{\partial}{\partial p}\left(\frac{f_0}{\sigma}\frac{\partial \Phi}{\partial p}\right)\right] \tag{6.26}$$

The three parts of (6.26), reading from left to right, are the *relative* vorticity, the *planetary* vorticity, and the *stretching* vorticity. As a parcel moves about in the atmosphere, the relative vorticity, planetary vorticity, and stretching vorticity terms may each change. But according to (6.25) their sum is conserved following the geostrophic motion. The scalar q, commonly called the quasi-geostrophic potential vorticity, is proportional to a linearized form of the Ertel potential vorticity discussed in Section 4.3. However, unlike Ertel's potential vorticity, q has units of vorticity and is determined solely by the isobaric geopotential distribution. Note that whereas Ertel's potential vorticity is conserved following the total motion on an isentropic surface, q is conserved following the geostrophic motion on an isobaric surface. For this reason some authors prefer the term *pseudo-potential vorticity*. However, we will generally refer to q as the quasi-geostrophic potential vorticity.

The stretching vorticity portion of q can be interpreted by substituting from the hydrostatic equation (6.2) to give

$$\frac{\partial}{\partial p}\left(\frac{f_0}{\sigma}\frac{\partial \Phi}{\partial p}\right) = -Rf_0\frac{\partial}{\partial p}\left(\frac{T}{\sigma p}\right) = -f_0\frac{\partial}{\partial p}\left(\frac{T}{S_p}\right) \approx -\frac{f_0}{S_p}\frac{\partial T}{\partial p}$$

where we have used the fact that S_p [as defined below (6.5)] varies only slowly with height in the troposphere. Referring back to Fig. 4.7, it is clear that as an air column moves adiabatically from left to right in the figure it is stretched vertically through upward motion in the upper portion and downward motion in the lower portion of the column. Thus, the upper portion must cool and the lower portion warm adiabatically so that $\partial T/\partial p$ must increase, and the stretching vorticity term becomes increasingly negative. If the planetary vorticity changes are small, the relative vorticity must then become increasingly positive in order that q remain constant following the geostrophic motion.

Comparing (6.23) and (6.25), we see that term A in (6.23) is actually just the tendency of q. Thus, the tendency of quasi-geostrophic potential vorticity is proportional to minus the geopotential tendency. A local increase (decrease) in q is associated with trough (ridge) development. Since q is a conserved quantity following the geostrophic motion we can diagnose the tendency purely from the geostrophic advection of q. Furthermore, (6.25) shows that the tendency will be zero (i.e., the flow will be steady) provided that the geostrophic wind is everywhere parallel to lines of constant q. Given the distribution of Φ, (6.25) can be integrated in time to provide a forecast of the evolution of the Φ field. However, because $\mathbf{V}_g$ depends on the distribution of Φ, the equation is highly nonlinear and numerical methods must be used for obtaining solutions.

6.4 Diagnosis of Vertical Motion

Since ζ_g and $\mathbf{V}_g$ are both defined in terms of $\Phi(x, y, p, t)$, (6.19) can be used to diagnose the ω field provided that the fields of both Φ and $\partial\Phi/\partial t$ are known. The former is a primary product of operational weather analysis. However, since upper-level analyses are generally available only twice per day, the latter can only be crudely approximated from observations by taking differences over 12 hours. Despite this limitation, the vorticity equation method of estimating ω is usually more accurate than the continuity equation method discussed in Section 3.5.1. However, neither of these methods of estimating ω uses the information available in the thermodynamic energy equation. An alternative method of estimating the vertical motion that utilizes both the vorticity equation and the thermodynamic equation is developed in this section.

6.4.1 Omega Equation

If we eliminate χ instead of ω between equations (6.21) and (6.22) we obtain a diagnostic equation that relates the field of ω at any instant to the Φ field at the same time. This equation is called the vertical motion or *omega equation.* Unlike the vorticity equation or thermodynamic energy equation methods discussed earlier, the omega equation method of diagnosing the vertical velocity requires information on the geopotential distribution at only a single time. Furthermore, since the omega equation arises from a combination of the vorticity and thermodynamic equations, the values of ω determined are consistent with both equations.

To obtain the omega equation we take the horizontal Laplacian of (6.21) to yield

$$\nabla^2 \frac{\partial \chi}{\partial p} = -\nabla^2 \left[\mathbf{V}_g \cdot \nabla \left(\frac{\partial \Phi}{\partial p} \right) \right] - \sigma \nabla^2 \omega \tag{6.27}$$

We next differentiate (6.22) with respect to pressure, yielding

$$\frac{\partial}{\partial p}(\nabla^2 \chi) = -f_0 \frac{\partial}{\partial p} \left[\mathbf{V}_g \cdot \nabla \left(\frac{1}{f_0} \nabla^2 \Phi + f \right) \right] + f_0^2 \frac{\partial^2 \omega}{\partial p^2} \tag{6.28}$$

Since the order of the operators on the left-hand side in (6.27) and (6.28) may be reversed, the result of subtracting (6.27) from (6.28) is to eliminate χ. After some rearrangement of terms, we obtain the *omega equation*

$$\underbrace{\left(\nabla^2 + \frac{f_0^2}{\sigma} \frac{\partial^2}{\partial p^2} \right)}_{\text{A}} \omega = \frac{f_0}{\sigma} \frac{\partial}{\partial p} \underbrace{\left[\mathbf{V}_g \cdot \nabla \left(\frac{1}{f_0} \nabla^2 \Phi + f \right) \right]}_{\text{B}} + \underbrace{\frac{1}{\sigma} \nabla^2 \left[\mathbf{V}_g \cdot \nabla \left(-\frac{\partial \Phi}{\partial p} \right) \right]}_{\text{C}} \tag{6.29}$$

Equation (6.29) involves only derivatives in space. It is, therefore, a diagnostic equation for the field of ω in terms of the instantaneous Φ field. The omega equation, unlike the continuity equation, provides a method of estimating ω that does not depend on observations of the ageostrophic wind. In fact, direct wind observations are not required at all, nor does the omega equation require information on the vorticity tendency, as required in the vorticity equation method, or on the temperature tendency, as required in the adiabatic method discussed in Section 3.5.2. Only observations of Φ at a single time are needed to determine the ω field using (6.29). The terms in (6.29), however, employ higher-order derivatives than are involved in the other methods of estimating ω. Accurately estimating such terms from noisy observational data can be quite difficult.

The terms in (6.29) can be physically interpreted in a manner analogous to the corresponding terms in the tendency equation. The differential operator in A is very similar to the operator in term A of the tendency equation (6.23). Thus, term A acts to spread the response to a localized forcing. Because the forcing in (6.29) tends to be a maximum in the midtroposphere and ω is required to vanish at the upper and lower boundaries, for qualitative discussion it is permissible to assume that ω has sinusoidal behavior not only in the horizontal but also in the vertical:

$$\omega = W_0 \sin(\pi p/p_0) \sin kx \sin ly$$

we can then write

$$\left(\nabla^2 + \frac{f_0^2}{\sigma} \frac{\partial^2}{\partial p^2} \right) \omega \approx -\left[k^2 + l^2 + \frac{1}{\sigma} \left(\frac{f_0 \pi}{p_0} \right)^2 \right] \omega$$

which shows that term A in (6.29) is proportional to $-\omega$. Recalling that ω is proportional to $-w$ so that $\omega < 0$ implies *upward* vertical motion, we see that term A is proportional to the vertical velocity. Thus, there will be upward (downward) motion where the sum of terms B and C is positive (negative). The physical significance of each of these forcing terms is discussed in turn below.

Term B is called the *differential vorticity advection.* Clearly this term is proportional to the rate of increase with height of the advection of absolute vorticity. To understand the role of differential vorticity advection we again consider an idealized developing baroclinic system. Figure 6.11 indicates schematically the geopotential contours at 500 and 1000 mb for such a system. At the centers of the surface high and surface low, designated H and L, respectively, the vorticity advection at 1000 mb must be very small. However, at 500 mb the positive relative vorticity advection is a *maximum* above the surface low, while negative relative vorticity advection is strongest above the surface high. Thus, for a short-wave system where relative vorticity advection is larger than the planetary vorticity advection the pattern of vertical motion owing to the influence of term B alone is

$$w \propto \begin{cases} \dfrac{\partial}{\partial z}[-\mathbf{V}_g \cdot \nabla(\zeta_g + f)] & \begin{matrix} <0 & \text{above point H} \\ >0 & \text{above point L} \end{matrix} \end{cases}$$

Thus, differential vorticity advection is associated with rising motion above the surface low and subsidence above the surface high. This pattern of vertical motion is in fact just what is required to produce the thickness tendencies in the 500–1000-mb layer above the surface highs and lows. For example, above the surface low there is positive vorticity associated with negative geopotential deviations since vorticity is proportional to the Laplacian of geopotential. Increasing vorticity thus implies a falling geopotential ($\chi < 0$). Hence the 500–1000-mb thickness is decreasing in that region. Since horizontal temperature advection is small above the center of the surface low, the only way to cool the atmosphere as required by the thickness tendency is by adiabatic cooling through the vertical motion field. Thus, the vertical motion maintains a hydrostatic temperature field (that is, a field in which temperature and thickness are proportional) in the presence of differential vorticity advection. Without this compensating vertical motion

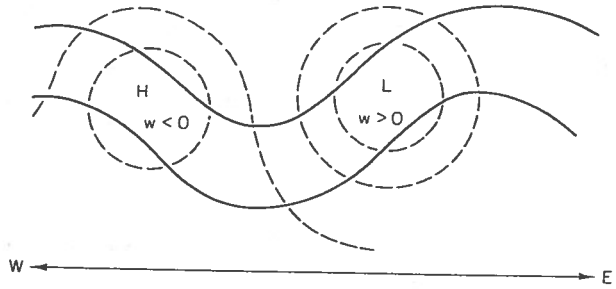

Fig. 6.11 Schematic 500-mb contours (solid lines) and 1000-mb contours (dashed lines) indicating regions of strong vertical motion owing to differential vorticity advection.

either the vorticity changes at 500 mb could not remain geostrophic or the temperature changes in the 500–1000-mb layer could not remain hydrostatic.

Term C of (6.29), which is merely the negative of the horizontal Laplacian of the thickness advection, is proportional to the thickness advection. The vertical velocity forced by term C acting alone is given by

$$w \propto \nabla^2\left[\mathbf{V}_g \cdot \nabla\left(-\frac{\partial \Phi}{\partial p}\right)\right] \propto -\mathbf{V}_g \cdot \nabla\left(-\frac{\partial \Phi}{\partial p}\right)$$

If there is warm (cold) advection, term C will be positive (negative) so that in the absence of differential vorticity advection w would be positive (negative). Thus, as indicated in Fig. 6.12, rising motion will occur to the east of the surface low in the warm front zone and sinking motion will occur west of the surface low behind the cold front. Physically, this vertical motion pattern is required to keep the upper-level vorticity field geostrophic in the presence of the height changes caused by the thermal advection. For example, warm advection increases the 500–1000-mb thickness in the region of the 500-mb ridge. Thus, the geopotential height rises at the ridge and the anticyclonic vorticity must increase if geostrophic balance is to be maintained. Since vorticity advection cannot produce additional anticyclonic vorticity at the ridge, horizontal divergence is required to account for the negative vorticity tendency. Continuity of mass then requires that there be upward motion to replace the diverging air at the upper levels. By analogous arguments it can be shown that subsidence is required in the cold advection region beneath the 500-mb trough.

To summarize, we have shown as a result of scaling arguments that for synoptic-scale motions where vorticity is constrained to be geostrophic and

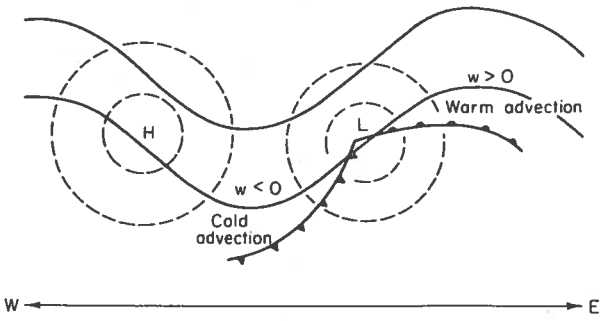

Fig. 6.12 Schematic 500-mb contours (thin solid lines), 1000-mb contours (dashed lines), and surface fronts (heavy lines) indicating regions of strong vertical motion owing to temperature advection.

temperature is constrained to be hydrostatic, the vertical motion field is determined uniquely by the geopotential field. Further, we have shown that this vertical motion field is just what is required to ensure that changes in vorticity will be geostrophic and changes in temperature will be hydrostatic. These constraints, whose importance can hardly be overemphasized, will be elaborated in the next subsection.

6.4.2 The Q Vector

Although terms B and C in the omega equation (6.29) apparently have clear interpretations as separate physical processes, in practice there is often a significant amount of cancellation between them. They also are not invariant under a Galilean transformation of the zonal coordinate. That is, adding a constant mean zonal velocity will change the magnitude of each of these terms without changing the net forcing of the vertical motion. For these reasons an alternative form of the omega equation, the **Q**-vector form, has been developed in which the forcing of the vertical motion is expressed in terms of the divergence of a horizontal vector forcing field.

In order to keep the mathematical development as simple as possible we will consider the **Q**-vector formulation of the omega equation only for the case in which β is neglected. This is usually referred to as an *f plane* because it is equivalent to approximating the geometry by a Cartesian planar geometry with constant rotation.

On the f plane the quasi-geostrophic prediction equations may be expressed simply as follows:

$$\frac{D_g u_g}{Dt} - f_0 v_a = 0 \tag{6.30}$$

$$\frac{D_g v_g}{Dt} + f_0 u_a = 0 \tag{6.31}$$

$$\frac{D_g T}{Dt} - S_p \omega = 0 \tag{6.32}$$

These are coupled by the thermal wind relationship

$$p\frac{\partial u_g}{\partial p} = \frac{R}{f_0}\frac{\partial T}{\partial y}, \qquad p\frac{\partial v_g}{\partial p} = -\frac{R}{f_0}\frac{\partial T}{\partial x} \tag{6.33a, b}$$

We now eliminate the time derivatives between (6.30) and (6.32) by first taking

$$p\frac{\partial}{\partial p}(6.30) - \frac{R}{f_0}\frac{\partial}{\partial y}(6.32)$$

to obtain

$$p\frac{\partial}{\partial p}\left[\frac{\partial u_g}{\partial t} + u_g\frac{\partial u_g}{\partial x} + v_g\frac{\partial u_g}{\partial y} - f_0 v_a\right] - \frac{R}{f_0}\frac{\partial}{\partial y}\left[\frac{\partial T}{\partial t} + u_g\frac{\partial T}{\partial x} + v_g\frac{\partial T}{\partial y} - S_p\omega\right] = 0$$

Using the chain rule of differentiation, this may be rewritten as

$$\frac{RS_p}{f_0}\frac{\partial \omega}{\partial y} - f_0 p\frac{\partial v_a}{\partial p} = -\left(\frac{\partial}{\partial t} + u_g\frac{\partial}{\partial x} + v_g\frac{\partial}{\partial y}\right)\left(p\frac{\partial u_g}{\partial p} - \frac{R}{f_0}\frac{\partial T}{\partial y}\right)$$
$$- p\left[\frac{\partial u_g}{\partial p}\frac{\partial u_g}{\partial x} + \frac{\partial v_g}{\partial p}\frac{\partial u_g}{\partial y}\right] + \frac{R}{f_0}\left[\frac{\partial u_g}{\partial y}\frac{\partial T}{\partial x} + \frac{\partial v_g}{\partial y}\frac{\partial T}{\partial y}\right]$$

But, by the thermal wind relation (6.33) the term in parenthesis on the right-hand side vanishes and

$$-p\left[\frac{\partial u_g}{\partial p}\frac{\partial u_g}{\partial x} + \frac{\partial v_g}{\partial p}\frac{\partial u_g}{\partial y}\right] = -\frac{R}{f_0}\left[\frac{\partial T}{\partial y}\frac{\partial u_g}{\partial x} - \frac{\partial T}{\partial x}\frac{\partial u_g}{\partial y}\right]$$

Using these facts, plus the fact that

$$\partial u_g/\partial x + \partial v_g/\partial y = 0$$

we finally obtain the simplified form

$$\sigma\frac{\partial \omega}{\partial y} - f_0^2\frac{\partial v_a}{\partial p} = -2Q_2 \tag{6.34a}$$

where

$$Q_2 \equiv -\frac{R}{p}\left[\frac{\partial u_g}{\partial y}\frac{\partial T}{\partial x} + \frac{\partial v_g}{\partial y}\frac{\partial T}{\partial y}\right] = -\frac{R}{p}\frac{\partial \mathbf{V}_g}{\partial y}\cdot\nabla T$$

Similarly, if we take

$$p\frac{\partial}{\partial p}(6.31) + \frac{R}{f_0}\frac{\partial}{\partial x}(6.32)$$

followed by application of (6.33b) we obtain

$$\sigma\frac{\partial\omega}{\partial x}-f_0^2\frac{\partial u_a}{\partial p}=-2Q_1 \tag{6.34b}$$

where

$$Q_1\equiv-\frac{R}{p}\left[\frac{\partial u_g}{\partial x}\frac{\partial T}{\partial x}+\frac{\partial v_g}{\partial x}\frac{\partial T}{\partial y}\right]=-\frac{R}{p}\frac{\partial\mathbf{V}_g}{\partial x}\cdot\nabla T$$

If we now take $\partial(6.34b)/\partial x+\partial(6.34a)/\partial y$ and use (6.12) to eliminate the ageostrophic wind, we obtain the **Q**-vector form of the omega equation:

$$\sigma\nabla^2\omega+f_0^2\frac{\partial^2\omega}{\partial p^2}=-2\nabla\cdot\mathbf{Q} \tag{6.35}$$

where

$$\mathbf{Q}\equiv(Q_1,Q_2)=\left(-\frac{R}{p}\frac{\partial\mathbf{V}_g}{\partial x}\cdot\nabla T,-\frac{R}{p}\frac{\partial\mathbf{V}_g}{\partial y}\cdot\nabla T\right) \tag{6.36}$$

Equation (6.35) shows that on the f plane vertical motion is forced only by the divergence of **Q**. Unlike the traditional form of the omega equation, the **Q**-vector form does not have forcing terms that partly cancel. The forcing of ω can be represented simply by the pattern of the **Q** vector. By the arguments of the last subsection the left-hand side in (6.35) is proportional to the vertical velocity (w). Hence, regions where **Q** is convergent (divergent) correspond to ascent (descent).

The **Q** vector may be interpreted physically by considering the special case of baroclinic motion that is purely geostrophic so that the vertical velocity vanishes. Then

$$\frac{D_gT}{Dt}=\left(\frac{\partial}{\partial t}+\mathbf{V}_g\cdot\nabla\right)T=0$$

Thus,

$$\frac{\partial}{\partial x}\left(\frac{\partial}{\partial t}+\mathbf{V}_g\cdot\nabla\right)T=\left(\frac{\partial}{\partial t}+\mathbf{V}_g\cdot\nabla\right)\frac{\partial T}{\partial x}+\frac{\partial\mathbf{V}_g}{\partial x}\cdot\nabla T=0$$

which implies that

$$\left(\frac{\partial}{\partial t}+\mathbf{V}_g\cdot\nabla\right)\frac{\partial T}{\partial x}=\frac{Q_1p}{R}$$

By symmetry,

$$\left(\frac{\partial}{\partial t}+\mathbf{V}_g\cdot\nabla\right)\frac{\partial T}{\partial y}=\frac{Q_2p}{R}$$

so that in vector form

$$\frac{D_g}{Dt}\left(\frac{R}{p}\nabla T\right)=\mathbf{Q} \tag{6.37}$$

Thus, **Q** is proportional to the rate of change of horizontal temperature gradient forced by geostrophic motion alone. By similar means it can be shown that the change in the vertical shear of the geostrophic wind owing to advection by purely geostrophic flow is given by

$$\frac{D_g}{Dt}\left(f_0\frac{\partial u_g}{\partial p}\right)=-Q_2,\qquad\frac{D_g}{Dt}\left(f_0\frac{\partial v_g}{\partial p}\right)=+Q_1 \tag{6.38}$$

Comparing (6.38) with the components of (6.37), we see that purely geostrophic flow will tend to destroy the thermal wind relationship since the forcing of the vertical shear of the geostrophic wind and the horizontal temperature gradient are equal in magnitude but have opposite signs. Only in the presence of ageostrophic winds and their accompanying vertical motions can the thermal wind balance be maintained.

Although (6.37) provides a useful physical interpretation of the **Q** vector, it is not easy to use this expression to estimate the direction and magnitude of the **Q** vector at a given point on a weather map. Such an estimate can be made quite readily, however, by utilizing an alternative expression for the **Q** vector. If the motion is referred to a Cartesian coordinate system in which the x axis is parallel to the local isotherm with cold air on the left, then (6.36) can be simplified to give

$$\mathbf{Q}=-\frac{R}{p}\left(\frac{\partial T}{\partial y}\right)\left(\frac{\partial v_g}{\partial x}\mathbf{i}-\frac{\partial u_g}{\partial x}\mathbf{j}\right)$$

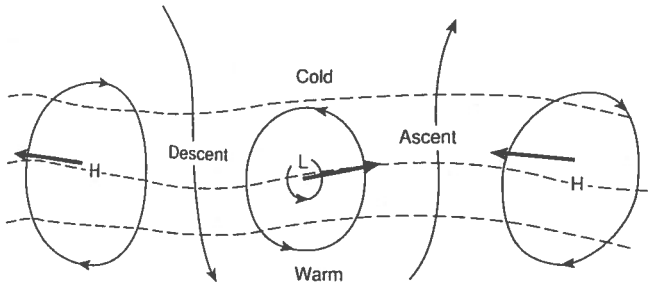

Fig. 6.13 Q vectors (bold arrows) for idealized pattern of isobars (solid) and isotherms (dashed) for a family of cyclones and anticyclones. (After Sanders and Hoskins, 1990.)

where we have again used the fact that $\partial u_g/\partial x = -\partial v_g/\partial y$. From the rules for cross multiplication of unit vectors the above expression for $\mathbf{Q}$ can be rewritten as

$$\mathbf{Q} = -\frac{R}{p}\left|\frac{\partial T}{\partial y}\right|\left(\mathbf{k}\times\frac{\partial \mathbf{V}_g}{\partial x}\right) \tag{6.39}$$

Thus, the $\mathbf{Q}$ vector can be obtained by evaluating the vectorial change of $\mathbf{V}_g$ along the isotherm (with cold air on the left), rotating the resulting change vector by 90° clockwise, and multiplying the resulting vector by $|\partial T/\partial y|$.

The $\mathbf{Q}$ vector, and hence the forcing of vertical motion, can be estimated with the aid of (6.39) from observations of Φ and T on a single isobaric surface. Examples for two simple cases, both of which have temperature decreasing toward the north, are shown in Figs. 6.13 and 6.14. Figure 6.13

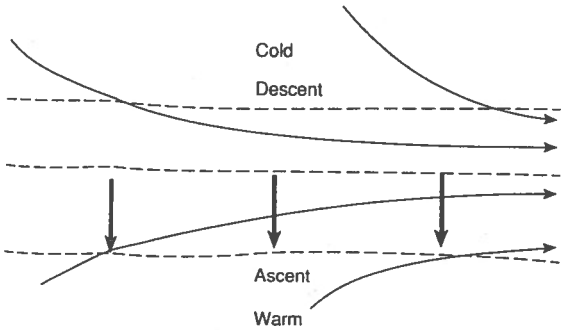

Fig. 6.14 Orientation of Q vectors (bold arrows) for confluent (jet entrance) flow. Dashed lines are isotherms. (After Sanders and Hoskins, 1990.)

shows an idealized pattern of cyclones and anticyclones in a slightly perturbed westerly thermal wind. Near the center of the low the geostrophic wind change moving eastward along the isotherm (i.e., with cold air to the left) is from northerly to southerly. Thus the geostrophic wind change vector points northward, and a 90° clockwise rotation produces a $\mathbf{Q}$ vector parallel to the thermal wind. In the highs, by the same reasoning the $\mathbf{Q}$ vectors are antiparallel to the thermal wind. The pattern of $\nabla\cdot\mathbf{Q}$ thus yields descent in the region of cold air advection west of the trough and ascent in the warm air advection region east of the trough.

In the situation shown in Fig. 6.14 the geostrophic flow is confluent so that the geostrophic wind increases eastward along the isotherms. In this case the vectorial change in $\mathbf{V}_g$ is parallel to the isotherms so that the $\mathbf{Q}$ vectors are normal to the isotherms and are directed up the temperature gradient. Again, rising motion occurs where the $\mathbf{Q}$ vectors are convergent. Since such rising must imply vorticity stretching in the column below, cyclonic vorticity will tend to increase below a region of upper level convergent $\mathbf{Q}$ vectors.

6.4.3 The Ageostrophic Circulation

In the traditional form of quasi-geostrophic theory given in Section 6.3 the ageostrophic velocity component is not explicitly determined. Rather, its role in the secondary vertical circulation is implicitly included through diagnostic determination of the ω vertical motion field. There are some dynamical aspects of the ageostrophic motion that are not, however, obvious from analysis of vertical motion alone. In particular, in some synoptic situations advection by the ageostrophic wind may be important in the evolution of the temperature and vorticity fields.

Since the ageostrophic wind generally has both irrotational and nondivergent components, the total ageostrophic flow field cannot be obtained from knowledge of the divergence alone. Rather, it is necessary to use the quasi-geostrophic momentum equation (6.11). If for simplicity we neglect the β effect and solve (6.11) for the ageostrophic wind we obtain

$$\mathbf{V}_a = \frac{1}{f_0}\mathbf{k}\times\frac{D_g\mathbf{V}_g}{Dt} = \frac{1}{f_0}\left[\mathbf{k}\times\frac{\partial \mathbf{V}_g}{\partial t} + \mathbf{k}\times(\mathbf{V}_g\cdot\nabla)\mathbf{V}_g\right] \tag{6.40}$$

which shows that in the Northern Hemisphere the ageostrophic wind vector is directed to the left of the geostrophic acceleration following the geostrophic motion.

The forcing of the ageostrophic wind can conveniently be divided into the two terms shown in brackets on the right in (6.40). The first term is

referred to as the *isallobaric* wind. It can easily be shown to be proportional to the gradient of the geopotential tendency (see Problem 6.13), and is directed down the gradient of the tendency field. This contribution to $\mathbf{V}_a$ is shown schematically for a baroclinic wave disturbance by the black arrows in Fig. 6.15. The second term in brackets in (6.40) may be called the advective part of the ageostrophic wind. For baroclinic waves in the jet stream the advective term is dominated by zonal advection so that

$$\mathbf{k}\times(\mathbf{V}_g\cdot\nabla)\mathbf{V}_g \approx \bar{u}\frac{\partial}{\partial x}(\mathbf{k}\times\mathbf{V}_g) = -f_0^{-1}\,\bar{u}\frac{\partial}{\partial x}(\nabla\Phi)$$

where $\bar{u}$ is the mean zonal flow, and we have used the definition of the

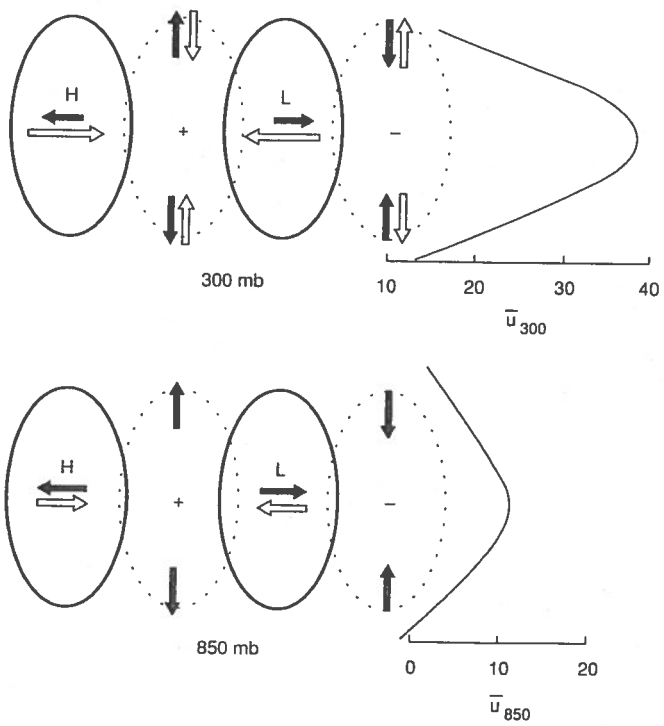

Fig. 6.15 Isallobaric and advective contributions to the ageostrophic wind for baroclinic waves in the westerlies. Solid ellipses indicate perturbation geopotential patterns at 300 and 850 mb. Dashed ellipses show geopotential tendency pattern with positive and negative tendencies indicated by + and − signs, respectively. The mean zonal flow distribution in which the waves are embedded is indicated on the right for each level. Solid arrows show the isallobaric part of the ageostrophic wind and open arrows show the advective part. (Adapted from Lim *et al.*, 1991.)

geostrophic wind (6.7). The advective contribution to the ageostrophic flow is shown by the open arrows in Fig. 6.15. Note that owing to the strong jet stream at 300 mb at the center of the waves the advective contribution dominates over the isallobaric contribution. On the flanks of the waves at 300 mb the two contributions are of comparable amplitude, so the net ageostrophic wind is small. At the 850-mb level, on the other hand, the two contributions nearly cancel at the center of the perturbations, while the advective contribution is nearly zero on the flanks. The net result is that the ageostrophic motion for baroclinic waves is primarily zonal in the upper troposphere and primarily meridional in the lower troposphere.

6.5 Idealized Model of a Baroclinic Disturbance

In Section 6.2 we showed that for synoptic-scale systems the fields of vertical motion and geopotential tendency are determined to a first approximation by the three-dimensional distribution of geopotential. The results of our diagnostic analyses using the geopotential tendency and omega equations can now be combined to illustrate the essential structural characteristics of a developing baroclinic wave. For reference, we restate here the qualitative content of the tendency and omega equations:

Geopotential Tendency Equation

$$\text{Geopotential}\begin{pmatrix}\text{fall}\\ \text{rise}\end{pmatrix} \propto \begin{pmatrix}+\\ -\end{pmatrix}\text{vorticity advection}$$

$$+\begin{pmatrix}\text{cold}\\ \text{warm}\end{pmatrix}\text{advection decreasing with height}$$

Omega Equation

$$\begin{pmatrix}\text{Rising}\\ \text{Sinking}\end{pmatrix}\text{motion} \propto \text{rate of increase with height of}\begin{pmatrix}+\\ -\end{pmatrix}\text{vorticity advection}$$

$$+\begin{pmatrix}\text{warm}\\ \text{cold}\end{pmatrix}\text{advection}$$

In Fig. 6.16 the relationship of the vertical motion field to the 500- and 1000-mb geopotential fields is illustrated schematically for a developing baroclinic wave. Also indicated are the physical processes that give rise to the vertical circulation in various regions.

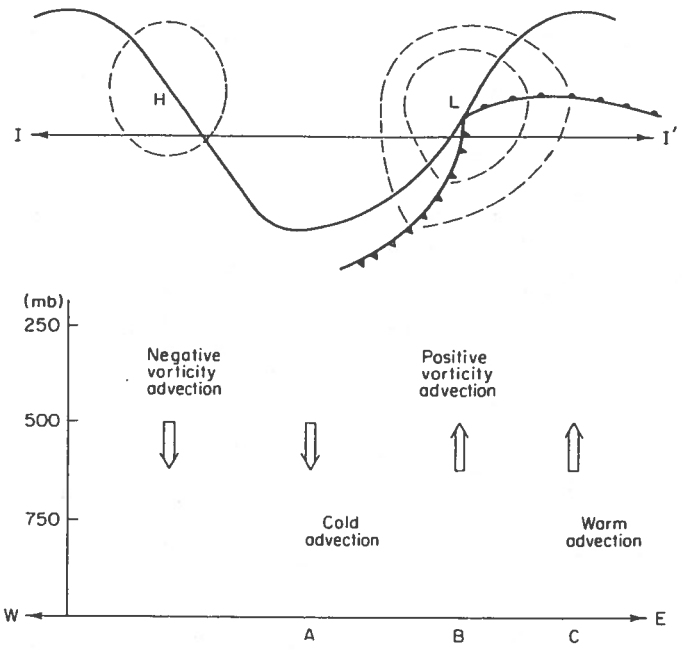

Fig. 6.16 Secondary circulation associated with a developing baroclinic wave: (top) schematic 500-mb contour (solid line), 1000-mb contours (dashed lines), and surface fronts; (bottom) vertical profile through the line II′ indicating the vertical motion field.

Additional structural features, including those that can be diagnosed with the tendency equation, are summarized in Table 6.1. In this table the signs of various physical parameters are indicated for vertical columns located at the position of (A) the 500-mb trough, (B) the surface low, and (C) the 500-mb ridge. It can be seen from this table that in all cases the vertical motion and divergence fields act to keep the temperature changes hydrostatic and vorticity changes geostrophic in order to preserve thermal wind balance.

Following the nomenclature of Chapter 5, we may regard the vertical and divergent ageostrophic motions as constituting a secondary circulation imposed by the simultaneous constraints of geostrophic and hydrostatic balance. The secondary circulation described in this chapter is, however, completely independent of the circulation driven by boundary layer pumping. In fact, it is observed that in midlatitude synoptic-scale systems, the vertical velocity forced by frictional convergence in the boundary layer is generally much smaller than the vertical velocity owing to differential vorticity advection. For this reason we have neglected boundary layer friction in developing the equations of the quasi-geostrophic system.

Table 6.1 *Characteristics of a Developing Baroclinic Disturbance*

Physical parameter	A 500-mb trough	B Surface low	C 500-mb ridge
$\partial(\delta\Phi)/\partial t$ (500–1000 mb)	Negative (thickness advection partly canceled by adiabatic warming)	Negative (adiabatic cooling)	Positive (thickness advection partly canceled by adiabatic cooling)
w (500 mb)	Negative	Positive	Positive
$\partial\Phi/\partial t$ (500 mb)	Negative (differential thickness advection)	Negative (vorticity advection)	Positive (differential thickness advection)
$\partial\zeta_g/\partial t$ (1000 mb)	Negative (divergence)	Positive (convergence)	Positive (convergence)
$\partial\zeta_g/\partial t$ (500 mb)	Positive (convergence)	Positive (advection partly canceled by divergence)	Negative (divergence)

It is also of interest to note that the secondary circulation in a developing baroclinic system always acts to oppose the horizontal advection fields. Thus, the divergent motions tend partly to cancel the vorticity advection and the adiabatic temperature changes owing to vertical motion tend to cancel partly the thermal advection. This tendency of the secondary flow to cancel partly the advective changes has important implications for the flow evolution. These will be discussed in Chapter 8.

It should now be clear that a secondary divergent circulation is necessary to satisfy the twin constraints of geostrophic and hydrostatic balance for a baroclinic system. Without such a circulation geostrophic advection tends to destroy the thermal wind balance. The secondary circulation is itself forced, however, by slight departures from geostrophy. Referring again to Fig. 6.16, we see that in the region of the upper-level trough (column A) cold advection causes the geopotential height to fall and thus intensifies the horizontal pressure gradient. The wind, therefore, becomes slightly subgeostrophic and experiences an acceleration across the isobars toward lower pressure. It is this cross-isobaric ageostrophic wind component that is responsible for the convergence that spins up the vorticity in the upper troposphere so that it adjusts geostrophically to the new geopotential distribution. In terms of the momentum balance, the cross-isobaric flow is accelerated by the pressure gradient force so that the wind speed adjusts back toward geostrophic balance. In the region of the upper-level ridge

analogous arguments apply, but in this case the ageostrophic flow leads to a divergent secondary circulation. In both cases, as we will see in Chapter 8, the ageostrophic flow toward lower pressure is associated with conversion of energy from potential energy to kinetic energy.

Problems

6.1. Show that the static stability parameter $\sigma = -\alpha\partial \ln \theta/\partial p$ may be written in terms of Φ as

$$\sigma = \frac{\partial^2\Phi}{\partial p^2} - \frac{1}{p}\frac{\partial\Phi}{\partial p}\left(\frac{R}{c_p} - 1\right) = \frac{1}{p^2}\left(\frac{\partial}{\partial \ln p} - \frac{R}{c_p}\right)\frac{\partial\Phi}{\partial \ln p}$$

6.2. Show that for an isothermal atmosphere σ, as defined in Problem 6.1, varies inversely as the square of the pressure.

6.3. Suppose that on the 50-kPa (500-mb) surface the relative vorticity at a certain location at 45°N latitude is increasing at a rate of $3\times10^{-6}\,s^{-1}$ per 3 h. The wind is from the southwest at $20\,m\,s^{-1}$ and the relative vorticity decreases toward the northeast at a rate of $4\times10^{-6}\,s^{-1}$ per 100 km. Use the quasi-geostrophic vorticity equation to estimate the horizontal divergence at this location on a β plane.

6.4. Given the following expression for the geopotential field:

$$\Phi = \Phi_0(p) + cf_0\{-y[\cos(\pi p/p_0)+1] + k^{-1}\sin k(x-ct)\}$$

where Φ_0 is a function of p alone, c is a constant speed, k a zonal wave number, and $p_0 = 100$ kPa (1000 mb):

(a) Use the quasi-geostrophic vorticity equation to obtain the horizontal divergence field consistent with this Φ field. (Assume that $df/dy = 0$.)

(b) Assuming that $\omega(p_0) = 0$, obtain an expression for $\omega(x, y, p, t)$ by integrating the continuity equation with respect to pressure.

(c) Sketch the geopotential fields at 75 kPa (750 mb) and 25 kPa (250 mb). Indicate regions of maximum divergence and convergence and positive and negative vorticity advection.

6.5. For the geopotential distribution of Problem 6.4 obtain an alternative expression for ω by using the adiabatic form of the thermodynamic energy equation (6.13). Assume that σ is a constant. For what value of k does this expression for ω agree with that obtained in Problem 6.4?

6.6. As an additional check on the results of Problems 6.4 and 6.5 use the omega equation (6.29) to obtain an expression for ω. Note that the three expressions for ω agree only for one value of k. Thus, the geopotential field $\Phi(x, y, p, t)$ of Problem 6.4 is consistent with quasi-geostrophic dynamics only for one value of the zonal wave number.

6.7. Suppose that the geopotential distribution at a certain time has the form

$$\Phi(x, y, p) = \Phi_0(p) - f_0U_0y\cos(\pi p/p_0) + f_0ck^{-1}\sin kx$$

where U_0 is a constant zonal speed and all other constants are as in Problem 6.4. Assuming that f and σ are constants, show by evaluating the terms on the right-hand side of the tendency equation (6.23) that $\chi = 0$ provided that $k^2 = \sigma^{-1}(f_0\pi/p_0)$.[2] Make qualitative sketches of the geopotential fields at 750 mb and 250 mb for this case. Indicate regions of maximum positive and negative vorticity advection at each level. (Note: the wavelength corresponding to this value of k is called the *radius of deformation.*)

6.8. For the geopotential field of Problem 6.7 use the omega equation (6.29) to find an expression for ω for the conditions in which $\chi = 0$. *Hint*: let $\omega = W_0\cos kx\sin(\pi p/p_0)$ where W_0 is a constant to be determined. Sketch a cross section in the x, p plane indicating trough and ridge lines, vorticity maxima and minima, vertical motion and divergence patterns, and locations of maximum cold and warm temperature advection.

6.9. Given the following expression for the geopotential field:

$$\Phi(x, y, p) = \Phi_0(p) + f_0[-Uy + k^{-1}V\cos(\pi p/p_0)\sin k(x-ct)]$$

where U, V, and c are constant speeds, use the quasi-geostrophic vorticity equation (6.19) to obtain an estimate of ω. Assume that $df/dy = \beta$ is a constant (*not zero*) and that ω vanishes for $p = p_0$.

6.10. For the conditions given in Problem 6.9, use the adiabatic thermodynamic energy equation to obtain an alternative estimate for ω. Determine the value of c for which this estimate of ω agrees with that found in Problem 6.9.

6.11. For the conditions given in Problem 6.9, use the omega equation (6.29) to obtain an expression for ω. Verify that this result agrees with the results of Problems 6.9 and 6.10. Sketch the phase relationship between Φ and ω at 250 mb and 750 mb. What is the amplitude of ω

if $\beta = 2\times10^{-11}\,\mathrm{m^{-1}\,s^{-1}}$, $U = 25\,\mathrm{m\,s^{-1}}$, $V = 8\,\mathrm{m\,s^{-1}}$, $k = 2\pi/(10^4\,\mathrm{km})$, $f_0 = 10^{-4}\,\mathrm{s^{-1}}$, $\sigma = 2\times10^{-6}\,\mathrm{Pa^{-2}\,m^2\,s^{-2}}$, and $p_0 = 10^2\,\mathrm{kPa}$?

6.12. Compute the **Q**-vector distributions corresponding to the geopotential fields given in Problems 6.4 and 6.7.

6.13. Show that the isallobaric wind may be expressed in the form

$$\mathbf{V}_{\mathrm{isall}} = -f_0^{-2}\nabla\chi$$

where $\chi = \partial\Phi/\partial t$.

Suggested References

Wallace and Hobbs, *Atmospheric Science: An Introductory Survey*, has an excellent description of the observed structure and evolution of midlatitude synoptic-scale disturbances.

Blackburn (1985) *Interpretation of ageostrophic winds and implications for jetstream maintenance*, discusses the differences between variable f(VF) and constant f(CF) ageostrophic motion.

Durran and Snellman (1987) illustrate the application of both the traditional and **Q**-vector forms of the omega equation in diagnosing the vertical motion of an observed system.

Sanders and Hoskins (1990) show how the distribution of **Q** vectors can easily be visualized on realistic weather maps.

Pedlosky, *Geophysical Fluid Dynamics, 2nd Edition*, presents a detailed formal derivation of the quasi-geostrophic system with applications to both the atmosphere and the oceans.

Chapter

7 Atmospheric Oscillations: Linear Perturbation Theory

In Chapter 13 we will discuss numerical techniques for solving the equations governing large-scale atmospheric motions. If the objective is to produce an accurate forecast of the circulation at some future time, a detailed numerical model based on the primitive equations and including processes such as latent heating, radiative transfer, and boundary layer drag should produce the best results. However, the inherent complexity of such a model generally precludes any simple interpretation of the physical processes that produce the predicted circulation. If we wish to gain physical insight into the fundamental nature of atmospheric motions, it is helpful to employ simplified models in which certain processes are omitted and compare the results with those of more complete models. This is, of course, just what was done in deriving the quasi-geostrophic model. However, the quasi-geostrophic potential vorticity equation is still a complicated nonlinear equation that must be solved numerically. It is difficult to gain an appreciation for the processes that produce the wavelike character observed in many meterological disturbances through study of numerical integrations alone.